

# EPJ E

Soft Matter and  
Biological Physics

EPJ.org  
your physics journal

Eur. Phys. J. E (2018) 41: 1

DOI 10.1140/epje/i2018-11607-x

## Membrane undulations in a structured fluid: Universal dynamics at intermediate length and time scales

Rony Granek and Haim Diamant

edp sciences



 Springer

# Membrane undulations in a structured fluid: Universal dynamics at intermediate length and time scales<sup>\*</sup>

Rony Granek<sup>1</sup> and Haim Diamant<sup>2,a</sup>

<sup>1</sup> The Stella and Avram Goren-Goldstein Department of Biotechnology Engineering, Ben-Gurion University of The Negev, Beer Sheva 84105, Israel

<sup>2</sup> Raymond & Beverly Sackler School of Chemistry, Tel Aviv University, Tel Aviv 69978, Israel

Received 18 August 2017 and Received in final form 4 December 2017

Published online: 5 January 2018 – © EDP Sciences / Società Italiana di Fisica / Springer-Verlag 2018

*This article is dedicated to the dear memory of Loïc Auvray, a colleague and friend whose wisdom was matched only by his kindness.*

**Abstract.** The dynamics of membrane undulations inside a viscous solvent is governed by distinctive, anomalous, power laws. Inside a viscoelastic continuous medium these universal behaviors are modified by the specific bulk viscoelastic spectrum. Yet, in structured fluids the continuum limit is reached only beyond a characteristic correlation length. We study the crossover to this asymptotic bulk dynamics. The analysis relies on a recent generalization of the hydrodynamic interaction in structured fluids, which shows a slow spatial decay of the interaction toward the bulk limit. For membranes which are weakly coupled to the structured medium we find a wide crossover regime characterized by different, universal, dynamic power laws. We discuss various systems for which this behavior is relevant, and delineate the time regime over which it may be observed.

## 1 Introduction

The main building block of biological membranes is a flexible fluid bilayer of phospholipid molecules [1]. Both the equilibrium and dynamic properties of this system have been vastly investigated (see, *e.g.*, refs. [2, 3]). As regards the linear response to out-of-plane forces, and the corresponding dynamics of fluctuations, most theoretical studies have considered membranes surrounded by a simple viscous solvent (*i.e.*, water) [4–9]. The strong fluctuations of tensionless membranes, along with the instantaneous response of the viscous solvent, result in anomalous dynamic exponents. The relaxation rate is much slower than that of an ordinary tension-dominated surface, scaling with wave number  $k$  as  $\Omega(k) \sim k^3$  rather than  $\sim k$ . The mean-square displacement (MSD) of a membrane segment in the transverse direction is subdiffusive, scaling with time  $t$  as  $\langle(\Delta h)^2(t)\rangle \sim t^{2/3}$  [10], between the confined fluctuations ( $\sim t^0$ ) of elastic surfaces, on the one hand, and normal dif-

fusion ( $\sim t$ ), on the other. The dynamic structure factor of membrane fluctuations follows a stretched-exponential decay,  $S(q, t) \sim \exp[-(\Gamma_q t)^{2/3}]$ , instead of the ordinary exponential decay in the case of normal diffusion [6].

Biological membranes, in particular, the plasma membrane of eukaryotic cells or the inner membrane of bacteria, however, are in contact with more complex media, such as the cytoskeleton or extra-cellular matrix. Artificial, self-assembled polymer-membrane complexes have been also thoroughly investigated [11–16]. The theory was extended, therefore, to membranes embedded in a viscoelastic medium [17]. In that work the medium was taken to be a structureless continuum, characterized by a complex frequency-dependent shear modulus  $G(\omega)$ . The specific frequency dependence of  $G(\omega)$  modifies the characteristic exponents of membrane dynamics into specific, medium-dependent ones.

Until recently, the bulk behavior of a continuous medium, as captured by  $G(\omega)$ , was thought to hold over distances larger than the medium's static correlation length  $\xi$  (*e.g.*, the mesh size of a polymer network). One of the first derivations of such “hydrodynamic screening” for semidilute flexible polymer solutions was that of Freed and Edwards, who found that the hydrodynamic

<sup>\*</sup> Contribution to “Polymers: From Adsorption to Translocation - Topical Issue in Memoriam Loïc Auvray (1956–2016)” edited by Jean-Marc Di Meglio, Fabien Montel, Jan C. Behrends.

<sup>a</sup> e-mail: hdiamant@tau.ac.il

interaction within the network decays as  $\exp(-r/\xi)/r$  at distances  $r \gg \xi$ , replacing the  $1/r$  Oseen interaction in a viscous fluid [18]. It has recently been discovered, however, that this description of hydrodynamic screening in structured fluids is lacking. The bulk behavior has been demonstrated, both experimentally and theoretically, to set in beyond a larger dynamic crossover distance [19–21],

$$\ell_c(\omega) = \xi [\eta(\omega)/\eta_s]^{1/2}, \quad (1)$$

where  $\eta(\omega) = G(\omega)/(i\omega)$ , and  $\eta_s$  is the shear viscosity of the solvent. Usually, over most of the relevant frequency range, one has  $\eta(\omega) \gg \eta_s$ , implying  $\ell_c \gg \xi$ . This opens up an intermediate spatio-temporal regime,  $\xi < r < \ell_c(\omega)$ , over which the dynamics of the medium is qualitatively different from its bulk behavior.

The purpose of the present work is to investigate the consequences of the distinct behavior within this intermediate regime for the dynamics of a membrane embedded in the structured fluid. To account for the dynamics of the fluid beyond its bulk behavior, we employ the two-fluid model of polymer networks [22–26].

In sect. 2 we present the model system under study. Subsequently, we begin the analysis in sect. 3 with a simple scaling argument, which qualitatively accounts for the basic effects (including power laws) to be derived in the sections that follow. The detailed analysis is divided into two stages. We first derive in sect. 4 the hydrodynamic interaction kernels, coupling the membrane with the two constituents of the surrounding fluid (polymer and solvent). The boundary conditions at the membrane surface define two limiting cases for the strength of the membrane-fluid coupling: a) weak coupling (sect. 4.1), where the membrane is in contact primarily with the solvent, and the network is affected indirectly, through its coupling to the solvent; b) strong coupling (sect. 4.2), where both solvent and network move together with the membrane. We then study in sect. 5 the consequences for the dynamics of membrane undulations—in particular, the transverse MSD of membrane segments (sect. 5.1). We examine the practical relevance of the general results for two examples of a structured fluid: a semidilute solution of flexible (sect. 5.2) and semiflexible (sect. 5.3) polymers. Finally, we discuss in sect. 6 the various findings, their limitations and implications.

## 2 Model

The system is schematically depicted in fig. 1. A tensionless membrane of bending rigidity  $\kappa$  is embedded in a medium made of a semidilute polymer network of mesh size  $\xi$  inside a solvent of viscosity  $\eta_s$ . We neglect the more detailed inner-membrane dynamics [5,8,9,27], which takes place on nanometric length scales. We use the spatial coordinates  $\mathbf{r} = (\boldsymbol{\rho}, z)$ , where  $\boldsymbol{\rho}$  is a two-dimensional (2D) position vector on the  $xy$ -plane. The membrane lies on average on the  $xy$ -plane and its out-of-plane configuration is parametrized by the height function  $h(\boldsymbol{\rho}, t)$ .

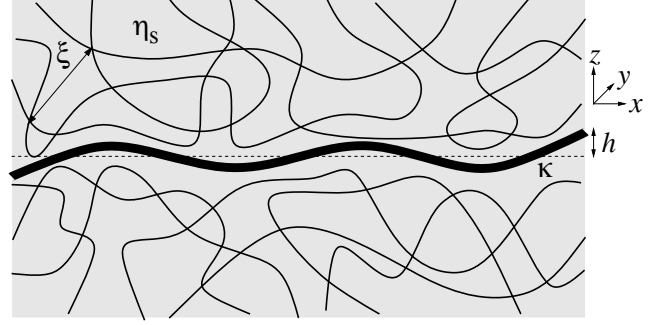


**Fig. 1.** Schematic illustration of the system and its parameters.

For the medium we use the two-fluid model, which is a well-studied model of polymer networks [21–26]. The model accounts for the response of the polymer network via viscoelastic shear and compression moduli,  $G_p(\omega)$  and  $K_p(\omega)$ , and for its coupling to the solvent via mutual friction with friction coefficient  $\Gamma(\omega)$ . The model yields the bulk shear viscosity as  $\eta(\omega) = G_p(\omega)/(i\omega) + \eta_s$ . It also produces two characteristic lengths. The first, emerging from the shear response, is given by  $\xi = [G_p\eta_s/(i\omega\Gamma)]^{1/2}$  and is identified with the mesh size<sup>1</sup>. The second is related to the compression response,  $\lambda = [(4G_p/3 + K_p)/(i\omega\Gamma)]^{1/2} = \xi[2(\eta/\eta_s)(1-\sigma)/(1-2\sigma)]^{1/2}$ , where  $\sigma$  is the network's Poisson ratio. The inequality  $\lambda/\xi > 1$  holds always, turning in the limit of an incompressible network ( $\sigma \rightarrow 1/2$ ) into  $\lambda/\xi \rightarrow \infty$ . From now on we are going to use the emergent parameters  $(\eta(\omega), \xi, \lambda)$ , instead of  $(G_p, K_p, \Gamma)$ .

Because of the two components in the two-fluid model, the hydrodynamic interactions are described by four tensorial kernels,  $\mathcal{G}_{pp}$ ,  $\mathcal{G}_{ss}$ ,  $\mathcal{G}_{ps}$ , and  $\mathcal{G}_{sp}$ . They correspond to the velocity response of each of the two components, polymer or solvent, to a force exerted on either the same or the other component—polymer-polymer, solvent-solvent, polymer-solvent, and solvent-polymer. Due to Onsager's reciprocal relations,  $\mathcal{G}_{ps} = \mathcal{G}_{sp}$ . The three tensors were calculated in ref. [26]. Of particular interest here is the solvent-solvent kernel. Asymptotically, for  $r \gg \xi$ , it is given by

$$\mathcal{G}_{ss}(\mathbf{r}) \simeq \frac{1}{8\pi\eta(\omega)r}(\mathbf{1} + \hat{r} \otimes \hat{r}) - \frac{\xi^2}{4\pi\eta_s r^3}(\mathbf{1} - 3\hat{r} \otimes \hat{r}). \quad (2)$$

This modified hydrodynamic interaction tensor, coupling two points located within the solvent, shows the crossover between the intermediate and bulk regimes at the distance  $\ell_c(\omega)$  as given by eq. (1). The first term, decaying as  $1/r$  and dominating at  $r \gg \ell_c$ , is the usual Oseen tensor. It governs the interaction at long distances and is controlled by the bulk viscoelasticity. The second term, decaying as  $1/r^3$ , dominates at  $\xi \ll r \ll \ell_c$  and depends on the much lower solvent viscosity. (A third, solvent-dominated regime at  $r \ll \xi$  is missing from this asymptotic expression.)

<sup>1</sup> The apparent frequency dependence of  $\xi$  is negligible so long as  $G_p \gg \eta_s\omega$ , *i.e.*, for frequencies that are not too high.

For actin networks, for example, the intermediate behavior was observed at distances of a few microns [19, 20].

It is important to note that the asymptotic two terms in eq. (2) reflect two conservation laws and, as such, do not depend on any specific model such as the two-fluid one [19, 21, 28]. The first term arises from momentum conservation of the entire medium; it describes the flow velocity due to the momentum monopole created by the force. The second term comes from mass conservation of the solvent as it flows past the network; it describes the flow due to the effective mass dipole created by the force over the mesh size  $\xi$ .

Because of its dipolar shape, the  $1/r^3$  term in eq. (2) vanishes identically under angular averaging. Thus, it does not affect properties such as the medium's dynamic structure factor or the pre-averaged correlation between two polymer segments. One is then left with the usual asymptotic (angle-averaged, diagonal) Oseen interaction  $1/(6\pi\eta r)$  [18]. In the present case, however, the nearly planar membrane breaks the isotropy of the system, and the  $1/r^3$  term contributes to the hydrodynamic interaction between membrane segments. As we shall see, this may change the crossover from solvent- to bulk-dominated dynamics of membrane undulations.

We tackle the problem from two different directions, both yielding identical results. In the first route, presented in the main text, we base the analysis on the 2D hydrodynamic kernel coupling two membrane segments. We obtain this kernel from the 3D kernels of the two-fluid model for two extreme situations. In one the polymer network is depleted from the membrane (weak-coupling limit), and in the other the polymer network is strongly adsorbed or anchored to the membrane (strong-coupling limit). In the second route, presented in the appendix, we study the membrane dynamics by solving a hydrodynamic boundary-value problem.

### 3 Scaling approach

We commence by presenting a simple scaling argument for the appearance of an intermediate dynamical regime of membrane undulations, assuming that the membrane interacts primarily with the solvent.

Consider two points on the membrane, separated by a projected distance  $\rho$ . Hydrodynamic interaction makes the transverse velocity of the membrane at one point,  $\partial h/\partial t$  respond to the transverse force density (per unit area)  $f$  exerted on it at the other point, as  $\partial h/\partial t = \Lambda(\rho)f$ . According to eq. (2), for  $\xi \ll \rho \ll \ell_c$ , the dominant hydrodynamic interaction obeys  $\Lambda(\rho) \sim \xi^2/(\eta_s \rho^3)$ . Its 2D Fourier transform is  $\Lambda(k) \sim \xi^2 k/\eta_s$ . Substituting the force density due to bending,  $f = \kappa \nabla^4 h$ , we obtain the relaxation rate of undulation mode  $\mathbf{k}$  as

$$\Omega(k) = \Lambda(k)\kappa k^4 \sim \kappa \xi^2 k^5/\eta_s. \quad (3)$$

Note the higher power law,  $\sim k^5$ , compared to the conventional  $\sim k^3$  law [4]. Let us assume, for the sake of the scaling argument, that the membrane size  $\ell$  is in the range

$\xi \ll \ell \ll \ell_c$ . Thus, the longest undulation relaxation time obeys

$$\tau(\ell) \sim [\Omega(k = \pi/\ell)]^{-1} \sim \eta_s \ell^5/(\kappa \xi^2). \quad (4)$$

We now assume the following scaling hypothesis for the transverse MSD of membrane segments,

$$\langle (\Delta h)^2(t) \rangle \equiv \langle (h(t) - h(0))^2 \rangle = \langle h^2 \rangle_{\text{eq}} \mathcal{U}(t/\tau(\ell)), \quad (5)$$

where  $\mathcal{U}(x)$  is a scaling function, and  $\langle h^2 \rangle_{\text{eq}}$  is the equilibrium mean-square undulation. As is well known [2, 3],  $\langle h^2 \rangle_{\text{eq}} \sim (k_B T/\kappa)\ell^2$ . Since the MSD should be independent of  $\ell$  for  $t \ll \tau(\ell)$ , it follows that the scaling function must behave as  $\mathcal{U}(x) \sim x^{2/5}$  for  $x \ll 1$ , leading to

$$\langle (\Delta h)^2(t) \rangle \sim (k_B T/\kappa)\xi^2(t/\tau_\xi)^{2/5}, \quad (6)$$

where  $\tau_\xi \simeq \eta_s \xi^3/\kappa$  is the undulation relaxation time of a membrane patch of size  $\xi$ . Thus,  $\langle (\Delta h)^2(t) \rangle \sim t^{2/5}$ , with a new anomalous diffusion exponent,  $2/5$ , replacing the conventional  $2/3$  exponent [6].

### 4 Hydrodynamic interaction kernel

As the first step in the detailed analysis, we calculate the 2D hydrodynamic-interaction kernel,  $\Lambda(\boldsymbol{\rho}, t)$ , correlating two points on the membrane in space and time. As the membrane lies on average on the  $xy$ -plane and fluctuates in the  $z$ -direction,  $\Lambda(\boldsymbol{\rho}, t)$  is generally obtained from a given 3D hydrodynamic kernel of the medium,  $\mathcal{G}_{ij}(\mathbf{r}, t)$ , as

$$\Lambda(\boldsymbol{\rho}, t) = \mathcal{G}_{zz}(\mathbf{r} = (\boldsymbol{\rho}, 0), t). \quad (7)$$

We use throughout this article Fourier transforms in 2D space,  $\boldsymbol{\rho} \rightarrow \mathbf{k}$  and in 3D space,  $\mathbf{r} \rightarrow \mathbf{q}$ , as well as Fourier-Laplace transforms in time,  $t \rightarrow \omega$ . The transformed 2D kernel is

$$\Lambda(\mathbf{k}, \omega) = \frac{1}{2\pi} \int_{-\infty}^{\infty} dq_z \mathcal{G}_{zz}(\mathbf{q} = (\mathbf{k}, q_z), \omega). \quad (8)$$

If the system is isotropic within the  $xy$ -plane, then  $\Lambda(\mathbf{k}, \omega) = \Lambda(k, \omega)$ .

For the two-fluid medium the situation is slightly more complicated. Consider a force density  $f$  in the  $z$ -direction, exerted by the membrane on the surrounding medium. Let us assume that a fraction  $\alpha$  of this force is exerted on the polymer network,  $f_p = \alpha f$ , and the rest is exerted on the solvent,  $f_s = (1 - \alpha)f$ . The transverse velocities of the two components at  $z = 0$  are then,

$$\begin{aligned} v_p(\mathbf{k}, \omega) &= [\alpha \Lambda_{pp}(\mathbf{k}, \omega) + (1 - \alpha) \Lambda_{ps}(\mathbf{k}, \omega)] f, \\ v_s(\mathbf{k}, \omega) &= [\alpha \Lambda_{sp}(\mathbf{k}, \omega) + (1 - \alpha) \Lambda_{ss}(\mathbf{k}, \omega)] f, \end{aligned} \quad (9)$$

where  $\{\Lambda_{ij}\}$  are 2D hydrodynamic kernels, and  $\Lambda_{ps} = \Lambda_{sp}$  from Onsager's reciprocity. To obtain  $\{\Lambda_{ij}\}$  we should substitute in eq. (8) the 3D kernels of the two-fluid model,  $\mathcal{G}_{pp}$ ,  $\mathcal{G}_{ss}$ , and  $\mathcal{G}_{ps} = \mathcal{G}_{sp}$  [26]. Performing the integration in eq. (8) gives

*see eqs. (10) on the next page*

$$A_{\text{pp}}(k, \omega) = \frac{1}{4\eta(\omega)k} \left[ 1 - 2\xi^2 k^2 \frac{\eta}{\eta_s} \left( 1 + \frac{\eta_s}{\eta} - \frac{1}{1 - \eta_s/\eta} \frac{\sqrt{1 + \lambda^2 k^2}}{\lambda k} + \frac{\eta_s/\eta}{\eta/\eta_s - 1} \frac{\xi k}{\sqrt{1 + \xi^2 k^2}} \right) \right], \quad (10a)$$

$$A_{\text{ss}}(k, \omega) = \frac{1}{4\eta(\omega)k} \left[ 1 + 2\xi^2 k^2 \left( \frac{\eta}{\eta_s} - 1 \right) \left( 1 - \frac{\xi k}{\sqrt{1 + \xi^2 k^2}} \right) \right], \quad (10b)$$

$$A_{\text{ps}}(k, \omega) = \frac{1}{4\eta(\omega)k} \left[ 1 - 2\xi^2 k^2 \left( 1 - \frac{\xi k}{\sqrt{1 + \xi^2 k^2}} \right) \right]. \quad (10c)$$

Over large distances the two components, polymer and solvent, move collectively as a single continuum [21]. Accordingly, in the limit  $k \ll \ell_c^{-1} < \xi^{-1}$ , eqs. (10) give  $A_{\text{pp}} \simeq A_{\text{ss}} \simeq A_{\text{ps}} \simeq 1/(4\eta(\omega)k)$ . Examining the solvent-solvent kernel in more detail, we find the following limiting behaviors:

$$A_{\text{ss}}(k, \omega) \simeq \begin{cases} \frac{1}{4\eta(\omega)k}, & k \ll \ell_c^{-1} \\ \frac{\xi^2 k}{2\eta_s}, & \ell_c^{-1} \ll k \ll \xi^{-1} \\ \frac{1}{4\eta_s k}, & k \gg \xi^{-1}, \end{cases} \quad (11)$$

displaying all three regimes: bulk, intermediate, and solvent-dominated. The expression in the intermediate regime agrees with the one used heuristically in sect. 3.

To apply the hydrodynamic kernels of eqs. (10) we need to know how the force exerted by the membrane is distributed between the two components of the surrounding medium. This will determine the effective kernel,  $\bar{\Lambda}(k, \omega)$ , governing membrane fluctuations. While the membrane is always in close contact with the solvent, its coupling to the polymer may be of different strengths. In the following two sub-sections we consider two limiting cases for the coupling strength.

#### 4.1 Weak coupling

Assume a polymer network that is inert to the membrane, such that only excluded-volume interactions exist between them. Consider eq. (9) for such a case. The mean fractions of membrane-polymer and membrane-solvent collisions are assumed to be  $\phi$  and  $(1 - \phi)$ , respectively, where  $\phi$  is the polymer volume fraction. This implies  $\alpha = \phi$  in eq. (9). Taking  $\phi \ll 1$ , and noting that for realistic parameters  $A_{\text{pp}}\phi \ll A_{\text{ps}}$  and  $A_{\text{sp}}\phi \ll A_{\text{ss}}$ , we have  $v_p \simeq A_{\text{ps}}f$  and  $v_s \simeq A_{\text{ss}}f$ . Since, in addition,  $A_{\text{ps}} \ll A_{\text{ss}}$ , this implies  $v_p \ll v_s$ , *i.e.*, the polymer moves much more slowly than the solvent. One concludes that the solvent moves with the membrane while the polymer is effectively frozen at some distance away. Thus, in this weak membrane-polymer coupling we may take

$$\bar{\Lambda}(k, \omega) \simeq A_{\text{ss}}(k, \omega). \quad (12)$$

In the alternative boundary-value formulation (see the appendix) we find that this limit is equivalent to assuming a no-slip boundary condition for the solvent and free

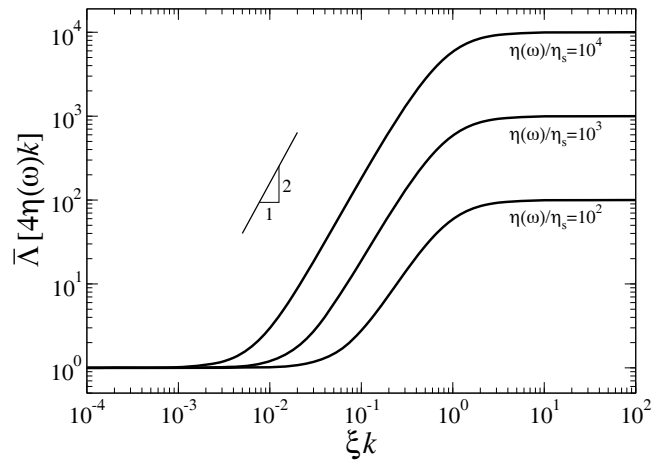


**Fig. 2.** Membrane hydrodynamic kernel in the weak-coupling limit. The kernel, normalized by its bulk ( $k \rightarrow 0$ ) expression, is plotted against the wave vector, normalized by the inverse mesh size of the network, at fixed frequency. In between the bulk limit (left-hand side) and the solvent-dominated limit (right-hand side) there is an intermediate region where  $\bar{\Lambda} \sim k$ . The width of this region increases with  $[\eta(\omega)/\eta_s]^{1/2}$  (curves from right to left).

(zero-stress) boundary condition for the polymer network. We will comment further on the physical relevance of this case in sect. 6. Note that the kernel in this limit is independent of  $\lambda$ , *i.e.*, of network compressibility (see eq. (10b)). This is because the membrane applies compressive stress exclusively on the solvent, and the network is displaced only due to the frictional coupling with the solvent. Figure 2 shows the weak-coupling kernel as a function of the wave vector, exhibiting the solvent-dominated, intermediate, and bulk regimes. The width of the intermediate regime is proportional to  $[\eta(\omega)/\eta_s]^{1/2}$ .

#### 4.2 Strong coupling

The other limit is that of strong coupling of the membrane to both solvent and polymer. This will be the case when the network is anchored, or strongly adsorbed, to the membrane. In this case we find the fraction  $\alpha$  in eq. (10) by demanding that the two components have the same

velocity at every point on the membrane at all times,  $\alpha A_{pp} + (1 - \alpha)A_{ps} = \alpha A_{sp} + (1 - \alpha)A_{ss} = \bar{A}$ . This gives

$$\alpha(k, \omega) = \left(1 - \frac{\eta_s}{\eta(\omega)}\right) \lambda k \times \frac{1 - \xi k(\sqrt{1 + \xi^2 k^2} - \xi k)}{(1 + \xi^2 k^2)\sqrt{1 + \lambda^2 k^2} - \xi \lambda k^2 \sqrt{1 + \xi^2 k^2}}. \quad (13)$$

Using eqs. (10b) and (10c), we obtain

$$\bar{A}(k, \omega) = \frac{1}{4\eta(\omega)k} \left[ 1 + 2\xi^2 k^2 \left( \frac{\eta(\omega)}{\eta_s} (1 - \alpha) - 1 \right) \times \left( 1 - \frac{\xi k}{\sqrt{1 + \xi^2 k^2}} \right) \right]. \quad (14)$$

An identical kernel to eq. (14) is obtained from the boundary-value formalism by imposing no-slip boundary conditions on both solvent and polymer (see the appendix).

A particularly simple limit is found for an incompressible polymer network, where eqs. (13) and (14) reduce to

$$\alpha(k, \omega) \xrightarrow{\lambda \rightarrow \infty} 1 - \frac{\eta_s}{\eta(\omega)} = \frac{G_p(\omega)}{G_p(\omega) + i\omega\eta_s},$$

$$\bar{A}(k, \omega) \xrightarrow{\lambda \rightarrow \infty} \frac{1}{4\eta(\omega)k}. \quad (15)$$

Thus, in this limit the force is everywhere distributed according to the relative resistance of the components to shear, and uniform viscoelasticity applies essentially at all wavelengths. This result is a consequence of the nearly planar membrane geometry, where the stress applied by the membrane is in the purely normal direction, *i.e.*, has only a  $zz$  component. (This is not true, for example, in the case of a sphere moving through the two-fluid medium [21].) Therefore, if both solvent and network are incompressible, they are bound to be displaced together by the  $zz$  stress, implying that the relevant viscosity everywhere is the collective one,  $\eta(\omega)$ .

The behavior just described suppresses the intermediate regime in the strong-coupling case even for compressible networks. To see this, we refine the criterion for eq. (15) to  $\lambda \gg \xi[\eta(\omega)/\eta_s]^{1/2} \sim \ell_c$ , corresponding to Poisson ratio  $|1/2 - \sigma| \ll 1$ . (This usually does not hold for polymeric networks.) In the large-wavelength regime,  $\lambda k \ll 1$ , where the polymer network is effectively compressible, we have  $\alpha \ll 1$  (see eq. (13)). This implies that  $\bar{A}(k, \omega) \simeq A_{ss}(k, \omega)$ ; yet, for such small  $k$ ,  $A_{ss}$  already behaves as the bulk kernel,  $A_{ss}(k, \omega) \simeq 1/(4\eta(\omega)k)$ , and the intermediate regime will not be observed. For  $\lambda \sim \ell_c$ , we expect some deviation from the limit of eq. (15) around  $\lambda k \sim \ell_c k \sim 1$ .

These observations are confirmed in fig. 3. Panel (a) shows the strong-coupling kernel as a function of  $k$ , for three different values of  $\eta(\omega)/\eta_s$  and Poisson ratio  $\sigma = 0.4$ . Note how close the kernel remains to its bulk limit, due to

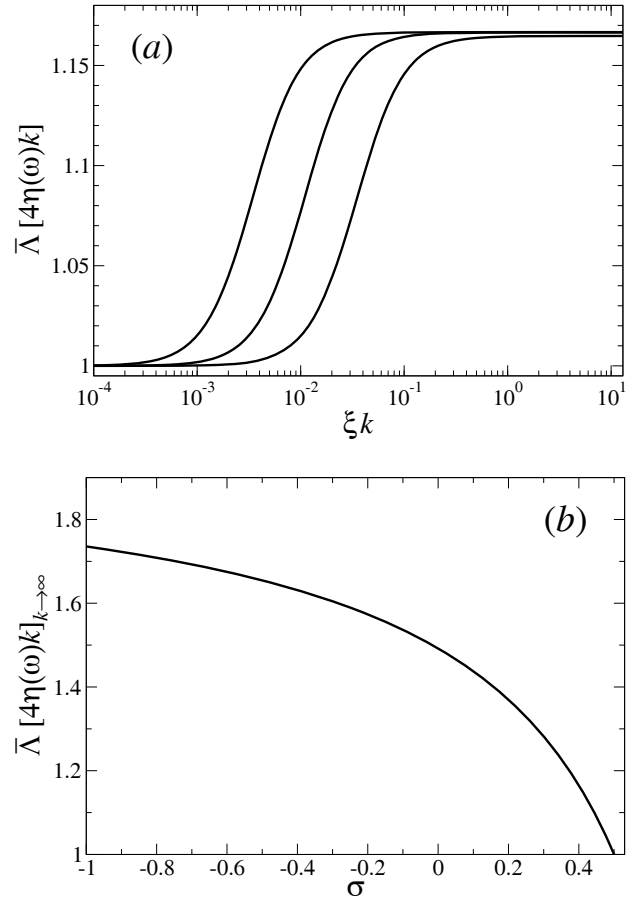


**Fig. 3.** (a) Membrane hydrodynamic kernel in the strong-coupling limit. The kernel, normalized by its bulk expression, is plotted against the wave vector, normalized by the inverse mesh size of the network, at fixed frequency, for Poisson ratio 0.4. The three curves, from right to left, correspond to  $\eta(\omega)/\eta_s = 10^2, 10^3$ , and  $10^4$ . (b) Large-wave-vector limit of the kernel as a function of Poisson ratio, for  $\eta(\omega)/\eta_s = 10^2$ . Note the narrow range of values (panel (a)), which completely disappears for  $\sigma = 1/2$  (panel (b)).

the response of the medium to compression. For the same reason the kernel exhibits neither the solvent-dominated behavior for  $\xi k \gg 1$  nor the intermediate region. The range of values narrows down to zero as the limit of incompressible network ( $\sigma = 1/2$ ) is approached. Figure 3(b) presents the large- $k$  limit of the kernel as a function of the Poisson ratio. The ratio between this small-scale limit and the bulk one remains of order 1 over the full range of Poisson ratios.

It is easy to generalize these results to the case of two different viscoelastic media (“1” and “2”) surrounding the membrane, as often occurs for biological membranes (*e.g.*, the cytoskeleton and the extra-cellular matrix). The half space (hf) interaction kernel for each side is twice that of the full space kernel,  $\bar{A}_i^{(hf)} = 2\bar{A}_i$ ,  $i = 1, 2$ . Distributing the membrane force between the two sides with fractions  $\beta$  and  $1 - \beta$ , and requiring that the membrane velocity be unique, we have  $\bar{A} = \bar{A}_1^{(hf)}\beta = \bar{A}_2^{(hf)}(1 - \beta)$ . This leads to

$\beta = \bar{A}_2^{(\text{hf})} / (\bar{A}_1^{(\text{hf})} + \bar{A}_2^{(\text{hf})})$ , and

$$\bar{A} = \frac{2\bar{A}_1\bar{A}_2}{\bar{A}_1 + \bar{A}_2}. \quad (16)$$

In the regimes where bulk viscoelasticity dominates in both media, this amounts to replacing  $\eta(\omega)$  by  $\eta_{\text{eff}} = [\eta_1(\omega) + \eta_2(\omega)]/2$ , which is a known result. Note however that the two media are not necessarily found in this regime together.

## 5 Membrane dynamics in a structured fluid

Given the hydrodynamic interaction kernel, as calculated in sect. 4, we may write down a generalized Langevin equation of motion for the membrane's displacement field  $h(\boldsymbol{\rho}, t)$  assuming small deformations [17],

$$\partial_t h(\boldsymbol{\rho}, t) = - \int_0^t dt' \int d^2\rho' \bar{A}(|\boldsymbol{\rho} - \boldsymbol{\rho}'|, t - t') \kappa \nabla_{\rho'}^4 h(\boldsymbol{\rho}', t') + \zeta(\boldsymbol{\rho}, t). \quad (17)$$

Here  $\zeta(\boldsymbol{\rho}, t)$  is a thermal colored noise, obeying the fluctuation-dissipation theorem,

$$\langle \zeta(\boldsymbol{\rho}, t) \zeta(\boldsymbol{\rho}', t') \rangle = k_B T \bar{A}(|\boldsymbol{\rho} - \boldsymbol{\rho}'|, |t - t'|). \quad (18)$$

Applying to eq. (17) a Fourier transform in  $\boldsymbol{\rho}$  and a Fourier-Laplace transform in  $t$  yields

$$i\omega h(\mathbf{k}, \omega) - h(\mathbf{k}, t = 0) = -\bar{A}(k, \omega) \kappa k^4 h(\mathbf{k}, \omega) + \zeta(\mathbf{k}, \omega). \quad (19)$$

Solving eq. (19) for  $h$ , we find

$$h(\mathbf{k}, \omega) = \frac{h(\mathbf{k}, t = 0) + \zeta(\mathbf{k}, \omega)}{i\omega + \Omega(k, \omega)}, \quad (20)$$

with the generalized relaxation rate,

$$\Omega(k, \omega) = \bar{A}(k, \omega) \kappa k^4. \quad (21)$$

Consider now the transverse MSD  $\langle (\Delta h)^2(t) \rangle$  and its Fourier-Laplace transform  $\langle (\Delta h)^2(\omega) \rangle$ . It can be conveniently written as [17]

$$\langle (\Delta h)^2(\omega) \rangle = \frac{1}{2\pi^2} \frac{k_B T}{\kappa} \int \frac{d^2k}{k^4} \left( \frac{1}{i\omega} - \frac{1}{i\omega + \Omega(k, \omega)} \right). \quad (22)$$

Rearranging the integrand using eq. (21) for  $\Omega$ , we have

$$\langle (\Delta h)^2(\omega) \rangle = \frac{1}{\pi} \frac{k_B T}{i\omega} \int_0^\infty dk \frac{k \bar{A}(k, \omega)}{i\omega + \bar{A}(k, \omega) \kappa k^4}. \quad (23)$$

The integral in eq. (23) is not easily evaluated analytically. We turn, therefore, to asymptotic analysis and numerical integration for several examples. As has been shown in sect. 4, strong membrane-network coupling suppresses the intermediate dynamics, leaving us with the already known solvent-dominated [6] and bulk [17] regimes. Hence, in what follows, we focus on the weak-coupling limit.

### 5.1 Transverse MSD of a weakly coupled membrane

Using  $A_{\text{ss}}$  of eq. (10b) in eq. (23) and transforming to a dimensionless wave number  $\hat{k} = k\xi$ , we obtain

$$\langle (\Delta h)^2(\omega) \rangle = A \int_0^\infty d\hat{k} \frac{\Psi(\hat{k}, \hat{\eta})}{1 + \hat{\gamma} \hat{k}^3 \Psi(\hat{k}, \hat{\eta})}, \quad (24)$$

where we have defined

$$A = \frac{k_B T}{4\pi(i\omega)^2 \eta(\omega) \xi},$$

$$\hat{\eta} = \frac{\eta(\omega)}{\eta_s} - 1,$$

$$\hat{\gamma} = \frac{\kappa}{4i\omega \eta(\omega) \xi^3},$$

$$\Psi(\hat{k}, \hat{\eta}) = 1 + 2\hat{\eta} \hat{k}^2 \left( 1 - \frac{\hat{k}}{\sqrt{1 + \hat{k}^2}} \right).$$

Studying the dependence of eq. (24) on  $\hat{\eta}$  and  $\hat{\gamma}$ , we find three asymptotic regimes:

- i) *Solvent-dominated regime*, which holds at high frequencies such that  $\hat{\gamma} \ll 1$  (more precisely,  $\hat{\gamma} \ll \hat{\eta}^{-1}$ ). Here the integral is dominated by  $\hat{k} \gg 1$  such that  $\Psi \simeq 1 + \hat{\eta}$ . This leads to

$$\langle (\Delta h)^2(\omega) \rangle = A \frac{2\pi}{3\sqrt{3}} (1 + \hat{\eta})^{2/3} \hat{\gamma}^{-1/3}, \quad (25)$$

or, in terms of dimensional parameters,

$$\langle (\Delta h)^2(\omega) \rangle = B_1 \frac{k_B T}{\kappa^{1/3} \eta_s^{2/3} (i\omega)^{5/3}}, \quad (26)$$

where  $B_1 = 2^{-1/3} 3^{-3/2} \simeq 0.153$ . This is the known result for a membrane embedded in a purely viscous solvent [6, 7].

- ii) *Intermediate regime*, holding for intermediate frequencies such that  $\hat{\eta}^{-1} \ll \hat{\gamma} \ll \hat{\eta}^{3/2}$ . Here the integral is dominated by  $\hat{\eta}^{-1/2} \ll \hat{k} \ll 1$ , such that  $\Psi \simeq 2\hat{\eta} \hat{k}^2$ . This leads to

$$\langle (\Delta h)^2(\omega) \rangle = A \frac{2^{9/10} \pi (\sqrt{5} - 1)^{1/2}}{5^{5/4}} \hat{\eta}^{2/5} \hat{\gamma}^{-3/5}, \quad (27)$$

or, assuming that in this regime  $\eta(\omega) \gg \eta_s$ ,

$$\langle (\Delta h)^2(\omega) \rangle = B_2 \frac{k_B T \xi^2}{\kappa^{3/5} \eta_s^{2/5} (i\omega)^{7/5}}, \quad (28)$$

with  $B_2 = 2^{1/10} (\sqrt{5} - 1)^{1/2} / 5^{5/4} \simeq 0.159$ . Importantly, the MSD in the intermediate regime is independent of the bulk viscosity  $\eta(\omega)$ , leaving the mesh size  $\xi$  as the only network property at play.

- iii) *Bulk regime*, which holds at low frequencies such that  $\hat{\gamma} \gg \hat{\eta}^{3/2}$ . Here the integral is dominated by  $\hat{k} \ll \hat{\eta}^{-1/2}$ , such that  $\Psi \simeq 1$ . This leads to

$$\langle (\Delta h)^2(\omega) \rangle = A \frac{2\pi}{3\sqrt{3}} \hat{\gamma}^{-1/3}, \quad (29)$$

or,

$$\langle(\Delta h)^2(\omega)\rangle = B_1 \frac{k_B T}{\kappa^{1/3} \eta(\omega)^{2/3} (i\omega)^{5/3}}, \quad (30)$$

which is the known result for a membrane embedded in a continuous viscoelastic medium [17].

In the time domain, the first two regimes become:

- i) *Solvent-dominated regime*, which holds at short times,  $t \ll \tau_\xi$ , where  $\tau_\xi = 4\eta_s \xi^3 / \kappa$  is the undulation relaxation time of a membrane patch of size  $\xi$ . In this regime,

$$\langle(\Delta h)^2(t)\rangle = B'_1 \left[ \left( \frac{k_B T}{\kappa} \right)^{\frac{1}{2}} \frac{k_B T}{\eta} t \right]^{2/3}, \quad (31)$$

where  $B'_1 = \Gamma[1/3] / (2\pi 4^{2/3}) \simeq 0.169$ .

- ii) *Intermediate regime*, which holds for intermediate times,  $\tau_\xi \ll t \ll \tau_c$ . The crossover time  $\tau_c$  is the solution of the equation

$$\tau_c = \tau_\xi \left( \frac{\eta[\omega = \tau_c^{-1}]}{\eta_s} \right)^{5/2}. \quad (32)$$

In this new regime

$$\langle(\Delta h)^2(t)\rangle = B'_2 \frac{k_B T \xi^2}{\kappa^{3/5} \eta_s^{2/5}} t^{2/5}, \quad (33)$$

where  $B'_2 = B_2 / \Gamma[7/5] \simeq 0.180$ . This result, up to the numerical prefactor, is the same as the one deduced from the scaling argument of sect. 3.

The time dependence in the third, bulk regime, as well as the crossover time  $\tau_c$  determining the width of the intermediate regime, depend on the specific bulk viscoelasticity. Generally, however, due to the power of 5/2 in eq. (32), the crossover time may be very long compared to  $\tau_\xi$ , yielding a broad intermediate regime. In the following two subsections we study two specific examples that demonstrate this behavior.

## 5.2 Membrane in a semidilute solution of flexible polymers

Let us take the weakly coupled network to be a semidilute flexible polymer solution. The network is characterized by the length  $L$  of the polymer chains, the entanglement length  $L_e$  (length of chain segments between entanglements), the mesh size  $\xi$ , and the intrinsic time scale  $\tau_0 = \eta_s \xi^3 / k_B T$ . The stress relaxation function is composed of four regimes [18, 29, 30]: i) Zimm/Rouse regime at short times,  $t < \tau_e$ , where  $\tau_e \simeq \tau_0$  is the entanglement time; ii) “breathing”-plateau regime at intermediate times,  $\tau_e < t < \tau_R$ , where  $\tau_R = \tau_e (L/L_e)^2$  is the Rouse time; iii) short-time reptation-plateau regime for  $\tau_R < t < \tau_{\text{rep}}$ , where  $\tau_{\text{rep}} = \tau_e (L/L_e)^3$  is the terminal (reptation) time; and iv) long-time reptation regime for  $t > \tau_{\text{rep}}$ .

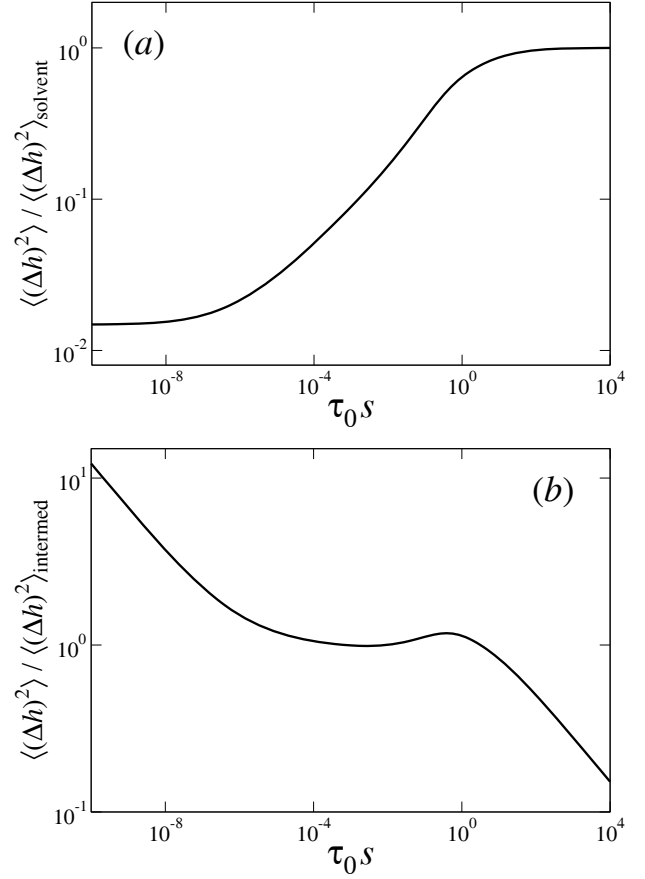


**Fig. 4.** Normalized MSD of a membrane in a flexible polymer network as a function of frequency  $s = i\omega$ . (a) The MSD is normalized by its solvent-dominated asymptote,  $\langle\Delta h^2\rangle_{\text{solvent}} \sim s^{-5/3}$  (eq. (26)). (b) The MSD is normalized by its intermediate-regime asymptote,  $\langle\Delta h^2\rangle_{\text{intermed}} \sim s^{-7/5}$  (eq. (28)). The frequency in both panels is normalized by  $\tau_0^{-1} = k_B T / (\eta_s \xi^3)$ . Parameters:  $\kappa / k_B T = 10$ ,  $L / \xi = 100$ ,  $L_e / \xi = 10$ .

Figure 4 shows the membrane’s transverse MSD for a strongly entangled case,  $L/L_e = 10$ , as a function of the frequency  $s = i\omega$ . These results were obtained by substituting the viscoelastic shear modulus accounting for the above regimes in eq. (24). We clearly see the two asymptotes,  $\sim s^{-5/3}$ , at small and large  $s$  values, and the intermediate regime,  $\sim s^{-7/5}$ , as predicted in sect. 5.1.

The intermediate regime spans 6–7 decades. Indeed, since the short and intermediate time behaviors have been argued above to be independent of the network’s complex modulus, the only relevant parameter is the crossover time  $\tau_c$ . A consistent solution of eq. (32) can be obtained only if the complex modulus is already in the long-time (small  $s$ ) reptation regime, *i.e.*, where the bulk is purely viscous, having an effective viscosity  $\eta(0) \sim \eta_s (L/L_e)^3$ . Solving for  $\tau_c$ , we find  $\tau_c \sim \tau_0 (L/L_e)^{15/2}$ , which is consistent with the wide frequency range shown in fig. 4. Obviously, we do not expect such a wide intermediate regime in reality; a smaller crossover time,  $t^* < \tau_c$ , arising from different physics, is expected to precede  $\tau_c$ , as will be discussed in sect. 6.

### 5.3 Membrane in a semidilute solution of semiflexible polymers

We now turn to the case of a membrane weakly coupled to a semidilute solution of semiflexible polymers, *e.g.*, an entangled F-actin network. Such a network has another intrinsic length—the polymer persistence length  $L_p$ . Assuming  $L_p \gg \xi$ , we have  $L_e \simeq \xi^{4/5} L_p^{1/5}$  [31]. The following hierarchy of time scales emerges [32, 33]: entanglement time,  $\tau_e = \tau_0(\xi/L_p)^{1/5}$ ; two relaxation times related to filament undulations,  $\tau_{\phi p} = \tau_0(L_p/\xi)^{3/5}$  and  $\tau_{\phi L} = \tau_0(L/L_p)^{7/5}(L/\xi)^{3/5}$ ; and reptation time,  $\tau_{\text{rep}} = \tau_0(L/\xi)^3$ . For actin networks, typically,  $\xi \sim 0.1 \mu\text{m}$ ,  $L_p \sim 10 \mu\text{m}$ , and  $L \sim 20 \mu\text{m}$ , yielding  $\tau_e \sim \tau_0 \sim 10^{-4}$  s,  $\tau_{\phi p} \sim 10^{-3}$  s,  $\tau_{\phi L} \sim 10^{-2}$  s, and  $\tau_{\text{rep}} \sim 10^3$  s. This hierarchy defines the following regimes for the frequency-dependent response of the network [32, 33]:

$$G(\omega) = i\omega\eta(\omega) \simeq bG_0 \times \begin{cases} (L_p/\xi)^{5/4}(i\omega\tau_0)^{3/4}, & \omega > \tau_e^{-1}, \\ (L_p/\xi)^{7/5}, & \tau_{\phi p}^{-1} < \omega < \tau_e^{-1}, \\ (L_p/\xi)^{17/10}(i\omega\tau_0)^{1/2}, & \tau_{\phi L}^{-1} < \omega < \tau_{\phi p}^{-1}, \\ (L_p/\xi)^{7/5}(L_p/L), & \tau_{\text{rep}}^{-1} < \omega < \tau_{\phi L}^{-1}, \\ (L_p/\xi)^{22/5}(L/L_p)^2(i\omega\tau_0), & \omega < \tau_{\text{rep}}^{-1}, \end{cases} \quad (34)$$

where  $G_0 = k_B T/\xi^3$ , and  $b \sim 0.1$  is a numerical prefactor.

Figure 5 shows the results for the membrane's MSD, obtained by substituting eq. (34) in eq. (24). The three limiting behaviors—solvent-dominated, intermediate, and bulk—are clearly seen, and the asymptotic power laws are again confirmed. As in the case of flexible polymers, we do not expect the extremely wide intermediate regime seen in fig. 5 to be realistic; see sect. 6.

## 6 Discussion

In this paper we have considered two limiting strengths of coupling between the membrane and polymer network. The weak-coupling limit corresponds to a polymer network that does not move together with the membrane but is merely dragged by the resulting solvent flow. In this limit we have discovered a new intermediate wavelength regime for the dispersion relation of membrane undulations, which is translated into an intermediate regime in time of the dynamics of membrane roughness. We have found that for both flexible and semiflexible semidilute polymer solutions this intermediate regime spans several orders of magnitude in time, until the bulk viscoelasticity takes over. Yet, it is likely that an earlier crossover should occur, upon which the weak-coupling limit is no longer valid.

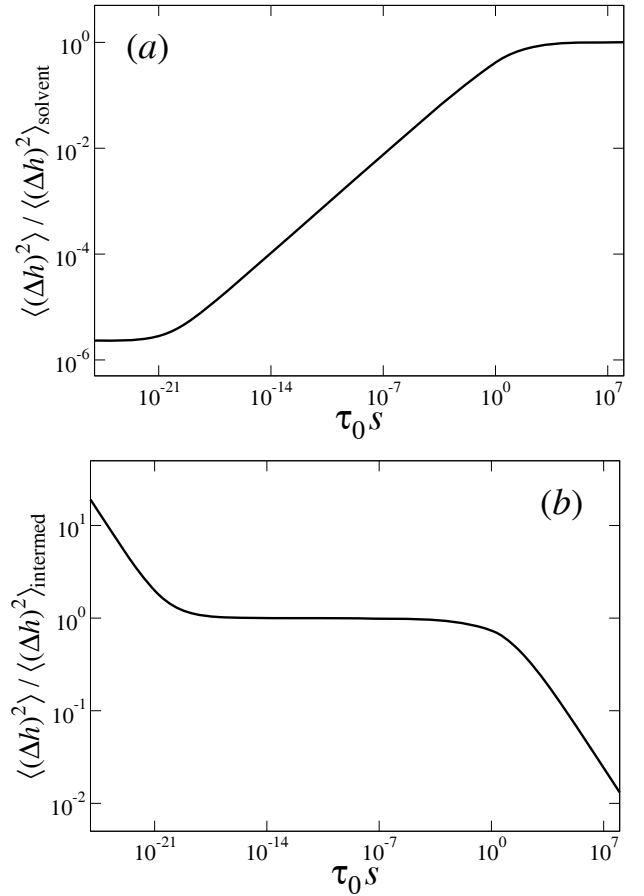


**Fig. 5.** Normalized MSD of a membrane in a semiflexible polymer network as a function of frequency  $s = i\omega$ . (a) The MSD is normalized by its solvent-dominated asymptote,  $\langle\Delta h^2\rangle_{\text{solvent}} \sim s^{-5/3}$  (eq. (26)). (b) The MSD is normalized by its intermediate-regime asymptote,  $\langle\Delta h^2\rangle_{\text{intermed}} \sim s^{-7/5}$  (eq. (28)). The frequency in both panels is normalized by  $\tau_0^{-1} = k_B T/(\eta_s \xi^3)$ . Parameters:  $\kappa/k_B T = 10$ ,  $L_p/\xi = 100$ ,  $L/\xi = 200$ .

To examine this issue, we first consider the thickness  $d$  of the depletion layer between the membrane and the polymer network. For both flexible and semiflexible polymers the network exerts on the membrane an osmotic pressure,  $\Pi_{\text{osm}} \sim k_B T/\xi^3$  [34]. The membrane exerts back on the network the well-known Helfrich repulsion [3],  $\Pi_{\text{Helf}} \sim (k_B T)^2/(\kappa d^3)$ . At equilibrium the two pressures balance each other, leading to  $d \sim (k_B T/\kappa)^{1/3}\xi$ . We assume that the weak-coupling limit is valid so long as the membrane's transverse MSD is smaller than  $d^2$ . When the MSD is larger, the polymer directly interacts with the membrane and a crossover to a different dynamics should take place. Equating eq. (6) with  $d^2$ , we infer the crossover time,

$$t^* \sim \left(\frac{\kappa}{k_B T}\right)^{5/6} \tau_\xi,$$

where  $\tau_\xi \sim \eta_s \xi^3/\kappa$ . This limits the intermediate  $t^{2/5}$  behavior of the MSD to  $\tau_\xi < t < t^*$ , suggesting that only for rigid membranes, where  $\kappa \sim 20\text{--}30 k_B T$ , should the intermediate regime be observed over a decade in time.

An interesting result can be obtained for a tense membrane or a surfactant-adsorbed oil-water interface in the weak-coupling limit. In the intermediate wavelength regime  $\ell_c^{-1} \ll k \ll (\xi^{-1}, \sqrt{\gamma/\kappa})$ , where  $\gamma$  is the surface tension, we have  $\Omega \simeq \Lambda(k)\gamma k^2 \simeq (\gamma\xi^2/\eta_s)k^3$ . Therefore, the membrane (or interface) undulation relaxation rate is equivalent to that of a tensionless membrane in a purely viscous and structureless fluid, with an effective bending rigidity,  $\kappa_{\text{eff}} = \gamma\xi^2$ . In experiments in which the relaxation rate of individual modes is aimed to be measured directly [16], this could make it hard to determine the physics behind an observation  $\Omega(k) \sim k^3$  without a counter measurement of the mean-square amplitude of thermally excited modes (which would be  $\approx k_B T / (\gamma k^2)$ ). For example, one could (wrongly) interpret such an observation as indicating membrane stiffening due to polymer adsorption. Yet, the relaxation rate of the dynamic structure factor is controlled by the (membrane segment) transverse MSD—which grows logarithmically with time, as for a membrane under tension in pure solvent [10]—suggesting that scattering experiments [14] could provide an efficient tool even in such delicate situations. From a different viewpoint, it has been argued that, for tensed membranes at long lengthscales, a crossover occurs to dynamics controlled by inter-monolayer friction, which could complicate further experimental interpretation [27].

Back to tensionless membranes in the weak-coupling limit, given that the intermediate regime is observed, our key predictions concerning its features are as follows: a) a dispersion relation  $\Omega \sim k^5$ ; b) MSD  $\sim t^{2/5}$ ; c) dynamic structure factor  $S(q, t) \sim \exp[-(\Gamma_q t)^\beta]$  and relaxation rate  $\Gamma_q \sim q^z$ , with  $\beta = 2/5$  and  $z = 5$ . To the best of our knowledge these universal predictions are yet to be observed in experiment [14–16]. Neutron spin echo measurements on a polymer-doped lamellar phase [14] showed a decrease of  $\beta$  and increase of  $z$  from their solvent-dominated values  $2/3$  and  $3$ , respectively, in a limited  $q$  range (see fig. 10 in ref. [14]). These results are suggestive but cannot be considered as a validation of our predictions. Other experimental systems such as polymer-filled liposomes [16] could be used to check the predictions.

We are grateful to the Telluride Science Research Center for its hospitality during a workshop where this work was initiated. We thank Shigeyuki Komura, Yael Roichman, Pierre Sens, and Matthiew Turner for helpful comments. HD has been supported by the Israel Science Foundation (Grant No. 164/14).

## Author contribution statement

Both authors contributed equally to this work.

## Appendix A. Boundary-value formulation

The problem of membrane dynamics inside a two-fluid medium can be formulated as a boundary-value problem for the medium. Apart from reproducing the results of

the hydrodynamic-kernel approach in the limits of weak and strong coupling (sect. 4), it allows the treatment of more elaborate boundary conditions, such as a network that slips at the membrane surface.

For simplicity we assume that the system is uniform along the  $y$ -axis. The remaining variables are  $(x, z, t)$ , turning, after applying a Fourier transform in  $x$  and a Fourier-Laplace transform in  $t$ , into  $(k, z, \omega)$ . The model then contains five  $z$ -dependent fields: the velocity  $(v_x, v_z)$  and pressure  $p$  of the solvent, and the displacement  $(u_x, u_z)$  of the polymer network.

The stresses in the two components (solvent and polymer) are given by

$$\begin{aligned}\sigma_{xx}^s &= -p + 2i\eta_s k v_x, \\ \sigma_{xz}^s &= \eta_s (\partial_z v_x + i k v_z), \\ \sigma_{zz}^s &= -p + 2\eta_s \partial_z v_z, \\ \sigma_{xx}^p &= i(K_p + 4G_p/3)k u_x + (K_p - 2G_p/3)\partial_z u_x, \\ \sigma_{xz}^p &= G_p (\partial_z u_x + i k u_x), \\ \sigma_{zz}^p &= (K_p + 4G_p/3)\partial_z u_z + i(K_p - 2G_p/3)k u_x.\end{aligned}\quad (\text{A.1})$$

The five equations for the five fields consist of four force-balance equations,

$$\begin{aligned}0 &= i k \sigma_{xx}^s + \partial_z \sigma_{xz}^s - \Gamma(v_x - i\omega u_x), \\ 0 &= i k \sigma_{xz}^s + \partial_z \sigma_{zz}^s - \Gamma(v_z - i\omega u_z), \\ 0 &= i k \sigma_{xx}^p + \partial_z \sigma_{xz}^p - \Gamma(i\omega u_x - v_x), \\ 0 &= i k \sigma_{xz}^p + \partial_z \sigma_{zz}^p - \Gamma(i\omega u_z - v_z),\end{aligned}\quad (\text{A.2})$$

and an incompressibility condition for the solvent (assuming a dilute polymer network),

$$0 = i k v_x + \partial_z v_z.\quad (\text{A.3})$$

Let us count the number of free coefficients to be matched by the number of boundary conditions. We divide each of the five fields into the two half-spaces on the two sides of the membrane,  $z < 0$  and  $z > 0$ , yielding ten  $z$ -dependent functions. The equations for the four  $v$ 's and four  $u$ 's are second order, and the ones for the two  $p$ 's are first order. We need, therefore, 18 boundary conditions. Ten are provided by demanding that all fields vanish at  $z \rightarrow \pm\infty$ . We are left with eight boundary conditions to be imposed at  $z = 0$  (the membrane surface). As usual, once these boundary conditions are stated, one obtains eight linear equations for the eight coefficients and, demanding the existence of a nontrivial solution, sets the secular determinant to zero. The resulting equation, linear in  $\omega$ , is readily solved for  $\omega$  to yield the dispersion relation,  $\Omega = -i\omega$ .

We choose to impose in all cases the following six boundary conditions (the  $\pm$  superscripts denote  $z \rightarrow 0^\pm$ , respectively, and  $\boldsymbol{\sigma} = \boldsymbol{\sigma}^s + \boldsymbol{\sigma}^p$  is the total stress):

- 1)  $0 = v_x^+ - v_x^-$ , continuity of tangential solvent velocity.
- 2)  $0 = v_z^+ - v_z^-$ , continuity of normal solvent velocity. The solvent sticks to the membrane; hence,  $v_z^\pm$  is also equal to the membrane's normal velocity,  $i\omega h$ .
- 3)  $0 = u_x^+ - u_x^-$ , continuity of tangential polymer displacement.

- 4)  $0 = u_z^+ - u_z^-$ , continuity of normal polymer displacement.  
 5)  $0 = \sigma_{xz}^+ - \sigma_{xz}^-$ , continuity of tangential stress.  
 6)  $0 = \sigma_{zz}^+ - \sigma_{zz}^- - \kappa k^4 v_z^-$ , balance of normal forces.

The remaining two boundary conditions vary according to the boundary conditions for the polymer network.

*Free network.* In this case the tangential and normal stresses exerted by the network both vanish. The two additional boundary conditions are, therefore,

- 7)  $0 = \sigma_{xz}^{p-} - \sigma_{xz}^{p+}$ , implying that the stresses entering condition (5) are exclusively the solvent's.  
 8)  $0 = \sigma_{zz}^{p-} - \sigma_{zz}^{p+}$ , implying that the stresses entering condition (6), balancing the membrane's bending force, are exclusively the solvent's.

The resulting dispersion relation is  $\Omega(k, \omega) = \kappa k^4 \bar{\Lambda}(k, \omega)$ , where  $\bar{\Lambda}$  is the kernel obtained in sect. 4 for the weak-coupling limit, eq. (10b).

*Sticking network.* In this case the network velocity at the membrane is equal to the solvent velocity there (and their normal components are both equal to the membrane's normal velocity). The boundary conditions are

- 7)  $0 = v_x^- - i\omega u_x^-$ , and the same holds for the “+” side due to conditions (1) and (3).  
 8)  $0 = v_z^- - i\omega u_z^-$ , and the same holds for the “+” side due to conditions (2) and (4).

The resulting dispersion relation is  $\Omega(k, \omega) = \kappa k^4 \bar{\Lambda}(k, \omega)$ , where  $\bar{\Lambda}$  is the kernel obtained in sect. 4.2 for the strong-coupling limit, eq. (14).

*Slipping network.* In this case the normal component of the network velocity at the membrane is equal to the solvent's (and both are equal to the membrane's), while the tangential stress exerted by the network vanishes,

- 7)  $0 = v_z^- - i\omega u_z^-$ , and the same holds for the “+” side due to conditions (2) and (4).  
 8)  $0 = \sigma_{xz}^{p-} - \sigma_{xz}^{p+}$ , implying that the tangential stresses entering condition (5) are exclusively the solvent's.

The resulting dispersion relation is

$$\Omega(k, \omega) = \frac{\kappa k^3}{4\eta(\omega)} \times \left[ 1 - 2(\eta/\eta_s - 1)k^2\xi^2 \left( 1 - \lambda k / \sqrt{1 + \lambda^2 k^2} \right) \right]^{-1}, \quad (\text{A.4})$$

which is always positive.

This result could not be obtained by the kernel approach used in the main text. This is because the slip condition does not set a condition for the relative velocities of the two components at the membrane, and, thus, cannot be used to determine the partition of force between the components, as has been done in sect. 4.

Clearly, other choices of boundary conditions can be similarly studied, such as partial slip between membrane and network, or asymmetric conditions (*e.g.*, network sticks to the membrane on one side and free on the other).

## References

1. B. Alberts *et al.*, *Essential Cell Biology*, 4th edition (Garland Science, 2013).
2. U. Seifert, *Adv. Phys.* **46**, 13 (1997).
3. S.A. Safran, *Statistical Thermodynamics Of Surfaces, Interfaces, and Membranes* (Westview Press, 2003).
4. F. Brochard, J.F. Lennon, *J. Phys. (Paris)* **36**, 1035 (1975).
5. U. Seifert, S.A. Langer, *Europhys. Lett.* **23**, 71 (1993).
6. A.G. Zilman, R. Granek, *Phys. Rev. Lett.* **77**, 4788 (1996).
7. A.G. Zilman, R. Granek, *Chem. Phys.* **284**, 195 (2002).
8. M.C. Watson, Y. Peng, Y. Zheng, F.L.H. Brown, *J. Chem. Phys.* **135**, 194701 (2011).
9. R.J. Bingham, S.W. Smye, P.D. Olmsted, *EPL* **111**, 18004 (2015).
10. R. Granek, *J. Phys. II* **7**, 1761 (1997).
11. R. Joannic, L. Auvray, D.D. Lasic, *Phys. Rev. Lett.* **78**, 3402 (1997).
12. E. Sackmann, M. Tanaka, *Trends Biotechnol.* **18**, 58 (2000).
13. M. Tanaka, E. Sackmann, *Nature* **437**, 656 (2005).
14. M. Mihailescu, M. Monkenbusch, J. Allgaier, H. Frielinghaus, D. Richter, *Phys. Rev. E* **66**, 041504 (2002).
15. R. Iniguez-Palomares, H. Acuna-Campa, A. Maldonado, *Phys. Rev. E* **84**, 011604 (2011).
16. F.-C. Tsai, B. Stuhmann, G.H. Koenderink, *Langmuir* **27**, 10061 (2011).
17. R. Granek, *Soft Matter* **7**, 5281 (2011).
18. M. Doi, S.F. Edwards, *The Theory of Polymer Dynamics* (Clarendon Press, 1988).
19. A. Sonn-Segev, A. Bernheim-Grosswasser, H. Diamant, Y. Roichman, *Phys. Rev. Lett.* **112**, 088301 (2014).
20. A. Sonn-Segev, A. Bernheim-Grosswasser, Y. Roichman, *Soft Matter* **10**, 8324 (2014).
21. H. Diamant, *Eur. Phys. J. E* **38**, 32 (2015).
22. P.-G. de Gennes, *Macromolecules* **9**, 587 (1976).
23. P.-G. de Gennes, *Macromolecules* **9**, 594 (1976).
24. M. Doi, A. Onuki, *J. Phys. II* **2**, 1631 (1992).
25. S.T. Milner, *Phys. Rev. E* **48**, 3674 (1993).
26. A.J. Levine, T.C. Lubensky, *Phys. Rev. E* **63**, 041510 (2001).
27. J.-B. Fournier, *Int. J. Nonlinear Mech.* **75**, 67 (2015).
28. H. Diamant, *Isr. J. Chem.* **47**, 225 (2007).
29. M. Rubinstein, E. Colby, *Polymer Physics* (Oxford, 2003).
30. R. Granek, M.E. Cates, *J. Chem. Phys.* **96**, 4758 (1992).
31. C.P. Broedersz, F.C. MacKintosh, *Rev. Mod. Phys.* **86**, 995 (2014).
32. F. Gittes, F.C. MacKintosh, *Phys. Rev. E* **58**, R1241 (1998).
33. D.C. Morse, *Macromolecules* **31**, 7044 (1998).
34. P.-G. de Gennes, *Scaling Concepts in Polymer Physics* (Cornell University Press, 1979).